

## A simple equation for determining sea surface emissivity in the 3–15 $\mu\text{m}$ region

R. NICLÒS\*†‡, V. CASELLES‡, E. VALOR‡, C. COLL‡ and J. M. SÁNCHEZ†‡

†Fundación Centro de Estudios Ambientales del Mediterráneo-CEAM (Mediterranean Centre for Environmental Studies), 14 Charles Darwin, E-46980 Paterna, Valencia, Spain

‡Department of Earth Physics and Thermodynamics, Faculty of Physics, University of Valencia, 50 Dr. Moliner, E-46100 Burjassot, Valencia, Spain

(Received 5 July 2006; in final form 10 October 2008)

The high level of accuracy demanded for the sea surface temperature retrieval from infrared data requires an accurate determination of directional sea surface emissivity (SSE). Previous models have permitted calculating SSEs using a physical characterization of sea surface roughness and emission. However, these result in complex equations, and make an operational application difficult. This paper presents a simple SSE algorithm based on a parametrization of one of these models, which was selected as a reference since it reproduces SSE experimental data to a reasonable level of accuracy. The parametrization provides the SSE variation with observation angle and wind speed from a given nadir SSE value, using only one channel-dependent coefficient. This coefficient and the nadir SSE value are given for the IR bands of several current satellite sensors: ENVISAT-AATSR, EOSTerra/Aqua-MODIS, NOAA17-AVHRR and MSG-SEVIRI. The average standard error of the SSE estimate using the proposed equation is  $\pm 0.0009$ .

### 1. Introduction

The accuracy currently required for the sea surface temperature (SST) determination for applications in climate monitoring and operational oceanography is  $\pm 0.3$  K, as defined by the International Tropical Ocean Global Atmosphere (TOGA) program (Barton 1992). This accurate SST retrieval demands an accurate determination of the sea surface emissivity (SSE) in the mid-wave and long-wave infrared (IR) regions for any observation geometry and sea surface roughness.

Several of the current and future satellite missions use IR observations at off-nadir viewing angles in the along-track direction, such as the Advanced Along Track Scanning Radiometer (AATSR) (Llewellyn-Jones *et al.* 2001) on board ENVISAT with a forward observation of  $55^\circ$ . Moreover, the observation angles at the image edges of satellite sensors with wide swaths in the across-track direction are quite large. This is the case of polar-orbit satellite sensors, such as the Advanced Very High Resolution Radiometer (AVHRR/2 and AVHRR/3) on board NOAA 14–18 (NOAA 2006) and the Moderate Resolution Imaging Spectrometer (MODIS) on EOS Terra/Aqua (Barnes *et al.* 1998). The  $55^\circ$  scan angle of these instruments increases to approximately  $65^\circ$  at the surface due to the Earth's curvature. Additionally, even larger observation angles (up to about  $75^\circ$ ) are used by the geostationary satellites,

---

\*Corresponding author. Email: Raquel.Niclos@uv.es

such as the Spinning Enhanced Visible and Infrared Imager (SEVIRI) on board Meteorol Second Generation (MSG) (Aminou *et al.* 1999). At these large viewing angles, the SSE shows a significant decrease from the value at nadir. For instance, there is an SSE reduction of about 1.5% at 11  $\mu\text{m}$  and of 2.4% at 12  $\mu\text{m}$  from 0° to 55°, as shown by experimental data (Smith *et al.* 1996, Nicolòs *et al.* 2005) and models (Masuda *et al.* 1988, Watts *et al.* 1996, Wu and Smith 1997). This fact must be taken into account for SST retrieval from satellite observations at large angles, since this SSE decrease leads to a significant SST error, e.g. about  $-1.2\text{ K}$  around 55° (François and Ottlé 1994). Therefore, an accurate determination of SSE is needed at these angles. In addition, SSE must account for wind speed, which causes an increase in the roughness of the sea surface, and has an important effect on SSE at a macro level (i.e. there is no change in the SSE of individual surface wave facets, since each one can be considered as a plane surface) as a result of radiance reflections.

SSE estimates can be obtained by models such as those of Masuda *et al.* (1988) and Wu and Smith (1997). The problem with these models, which are based on a physical characterization of the sea surface roughness and emission, is that they are rather complex and therefore not useful for operational purposes. For this reason, it would be desirable to have an accurate algorithm with as simple a parametrization as possible. In this paper, we present a simple parametrization of the SSE dependence on both wind speed and observation angle in the atmospheric windows of the IR region (i.e. 3–5  $\mu\text{m}$ , 8–9  $\mu\text{m}$  and 10–12  $\mu\text{m}$ , approximately).

In the next section, the existing theoretical models for estimating the SSE are analysed, pointing out the theoretical basis of each one, their differences and their accuracies. Once the most accurate model is selected, the SSE dependence on observation angle, wavelength and wind speed are studied, and the equation for the SSE parametrization is proposed in §3. Section 4 includes the results for the IR channels of ENVISAT-AATSR, EOS Terra/Aqua-MODIS, NOAA-AVHRR and MSG-SEVIRI. Finally, the conclusions are summarized in §5.

## 2. Previous models

The SSE depends on: (i) the sea surface roughness, which is generated by the surface wind,  $U$ ; (ii) the complex refractive index,  $n$ , which varies with salinity and sea temperature; and (iii) the observation angle at which the sea surface radiance is measured. Additionally, it depends on other factors, such as the presence of foam (Nicolòs *et al.* 2007b), which appears only for wind speeds larger than 10  $\text{m s}^{-1}$  (Masuda *et al.* 1988), and oil slicks. On this basis, the model of Masuda *et al.* (1988) established: (i) the emission geometry, considering the rough sea surface to be composed of many facets whose slopes can be defined using a normal and isotropic Gaussian distribution with the surface wind; (ii) the effect of salinity on the refractive index; and (iii) the difference between the observation angle and the incident angle. The monochromatic effective emissivity is written in this model as (Masuda *et al.* 1988):

$$\tilde{\varepsilon}(n, \mu_e, U) = \frac{\frac{2}{\pi\sigma^2\mu_e} \int_0^1 \int_0^\pi \varepsilon(n, \chi) \cos \chi \mu_n^{-4} \exp(-\tan^2\theta_n/\sigma^2) d\mu_n d\phi}{\frac{2}{\pi\sigma^2\mu_e} \int_0^1 \int_0^\pi \cos \chi \mu_n^{-4} \exp(-\tan^2\theta_n/\sigma^2) d\mu_n d\phi}, \quad (1)$$

where  $\sigma^2 = 0.003 + 0.00512 U$  and  $\chi$  is the angle between the emission direction and the normal of a wave facet tangent, which are defined by the angles  $\theta_e$  and  $\theta_n$  respectively, where  $\mu_e = \cos\theta_e$  and  $\mu_n = \cos\theta_n$ ; and  $\varepsilon(n, \chi)$  is the emissivity for each facet, which can be obtained as:

$$\varepsilon(n, \chi) = 1 - \rho(n, \chi), \tag{2}$$

where  $\rho(n, \chi)$  is the total reflectivity. For an IR radiometer, this is a simple average value of the two polarization complex reflectances, which are provided for the air–sea interface by Fresnel’s formula as a function of the complex refractive index for the sea water,  $n$ .

The paper of Masuda *et al.* (1988) provided tabulated SSEs as a function of the observation angle and the surface wind speed for several wavelengths in the IR window regions, both for pure and sea water. These tabulated values have been widely used as a reference model for estimating SSE.

In a previous work (Nicolòs *et al.* 2005), we studied the SSE angular dependence using measurements carried out from a fixed oilrig in the Mediterranean as a part of the WInd and Salinity Experiment campaign (WISE) of the ESA’s Soil Moisture and Ocean Salinity (SMOS) mission. Emissivities were measured by a Cimel Electronique CE 312 radiometer (Legrand *et al.* 2000) from October to December 2000. SSEs were determined for observation angles up to  $65^\circ$  and wind speeds up to  $15 \text{ m s}^{-1}$ , with an accuracy of  $\pm 0.004$  (Nicolòs *et al.* 2005). The model of Masuda *et al.* (1988) was in agreement with the experimental data up to  $50^\circ$ . However, we found a discrepancy between the SSEs computed by this model and the SSE values measured for observation angles larger than  $50^\circ$ . This is in accordance with previous observations of Smith *et al.* (1996). The computed SSEs show a negative bias, which needs to be corrected to avoid SST errors for off-nadir viewings. The relative error introduced by the model of Masuda *et al.* (1988) was larger than  $\pm 1\%$  at  $65^\circ$  (see figure 1). However, a precision of at least  $\pm 0.5\%$  is required to obtain an SST precision of  $\pm 0.3 \text{ K}$  (Wu and Smith 1997).

The model of Wu and Smith (1997) reproduces the effective SSE for any wind speed and observation angle more accurately (see figure 1), even for angles larger than  $50^\circ$ . The difference between the SSE values obtained using this model and the experimental data were always lower than the measurement accuracy ( $\pm 0.004$ ), while the disparity between the measurements and the results of the model of Masuda *et al.* (1988) were more than four times larger than the experimental accuracy at  $65^\circ$ . Thus, the model of Wu and Smith (1997) is considered as the reference in the present study. Wu and Smith (1997) accounted for the contribution of the radiance emitted by the sea surface reflecting back on itself, which is significant at high observation angles and wind speed values. In order to take this effect into account, the  $\varepsilon(n, \chi)$  introduced in equation (1) was replaced by (Wu and Smith 1997):

$$\varepsilon'(n, \chi) = \varepsilon(n, \chi) + [1 - \varepsilon(n, \chi)]P(\theta_r)\bar{\varepsilon}(n, \mu_r), \tag{3}$$

where  $\varepsilon(n, \chi)$  is now the emissivity at a facet point given by equation (2);  $P(\theta_r)$  is the probability that radiance arriving at this point with a local zenith angle  $\theta_r$  originates from the sea surface, with this being a function of the roughness dimensions; and  $\bar{\varepsilon}(n, \mu_r)$  is the mean emissivity of the sea surface that contributes to the radiance emitted at this angle, where  $\mu_r = \cos\theta_r = 2\cos\chi\cos\theta_n - \cos\theta_e$ .

The reflected emission causes a higher SSE increase with wind speed, removing the negative bias shown by the model of Masuda *et al.* (1988). The spectral and angular dependence of the SSE given by the model of Wu and Smith (1997) can be observed in figure 2.

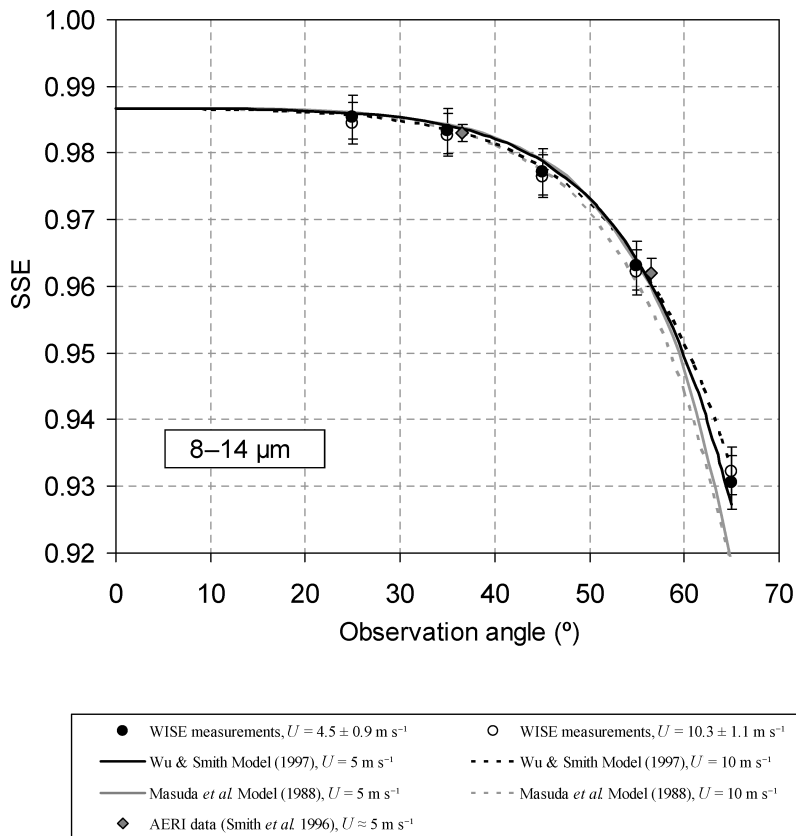


Figure 1. Angular variation of the sea surface emissivity (SSE). Comparison of experimental values (Niclòs *et al.* 2005) and theoretical SSEs computed by the model of Masuda *et al.* (1988) and the model of Wu and Smith (1997). Measurements with the Atmospheric Emitted Radiance Interferometer (AERI) (Smith *et al.* 1996) for wind speed,  $U$ , of about  $5 \text{ m s}^{-1}$  are also shown.

The model of Wu and Smith (1997) is a physical characterization of the sea surface emission, including the reflected emission, which explains its high level of accuracy. It is, however, mathematically complex. For this reason, in the next section we develop a simple algorithm, based on the values computed by the physical model of Wu and Smith (1997), to calculate accurate SSE as a function of wind speed and observation angle.

### 3. The algorithm

#### 3.1 A simple parametrization

The angular variation of SSE (see figures 1 and 2) suggested a parametrization in terms of a cosine function, but with a smaller decrease with angle, which could be attained by introducing additional coefficients. However, the higher complexity of the spectral dependence hinders a simple characterization of this spectral variability when using tables of SSE values at constant wavelength steps. Using as a reference the SSEs computed by van Delst and Wu (2000), following the model of Wu and Smith (1997) for wavelengths from 3 to  $16 \mu\text{m}$ , different

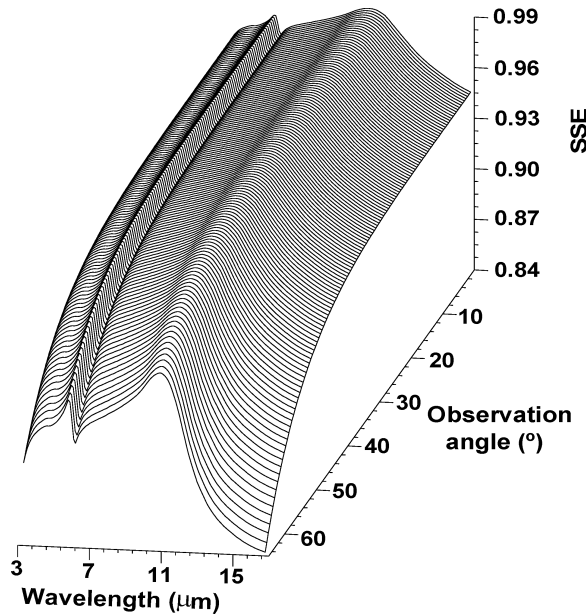


Figure 2. SSE dependence on wavelength and observation angle, as given by the model of Wu and Smith (1997) for a wind speed  $U=0 \text{ m s}^{-1}$ .

possible spectral fitting functions were tested. Finally, we concluded that the angular dependence could be adequately reproduced by an equation such as the following:

$$\varepsilon_{\lambda}(\theta, U) = \varepsilon_{\lambda}(0^{\circ}) \left[ \cos(\theta^{a_{\lambda}(U)}) \right]^{b_{\lambda}(U)}, \quad (4)$$

where  $\varepsilon_{\lambda}(\theta, U)$  is the spectral SSE as a function of the observation angle,  $\theta$  (radians) and the surface wind speed,  $U$  ( $\text{m s}^{-1}$ ), and where  $\varepsilon_{\lambda}(0^{\circ})$  is the corresponding SSE value at nadir, which has negligible dependence on surface wind speed (with a relative standard deviation lower than  $\pm 0.006\%$  for  $U$  values from 0 to  $15 \text{ m s}^{-1}$  (Masuda *et al.* 1988, Wu and Smith 1997, Niclòs *et al.* 2005)). The parameters  $a_{\lambda}(U)$  and  $b_{\lambda}(U)$  are the fitting coefficients, which, in principle, depend on both wavelength and surface wind speed.

The SSEs of the model of Wu and Smith (1997) (provided by van Delst and Wu (2000)) were spectrally fitted to equation (4) for wind speed values from 0 to  $15 \text{ m s}^{-1}$ , using the Levenberg–Marquardt non-linear least-squares algorithm (Moré 1977). Fit standard errors,  $\sigma_{f,\lambda}$ , lower than  $\pm 0.0009$  in emissivity were obtained for all cases. Figure 3 shows the spectral dependence of the  $a_{\lambda}(U)$  and  $b_{\lambda}(U)$  fitting coefficients for wind speed values of 0 and  $15 \text{ m s}^{-1}$ .

Note that  $a_{\lambda}(U)$  has a relative variation of  $\pm 19\%$  with  $U$ , but very little spectral variability is observed (lower than  $\pm 3\%$ ). On the other hand,  $b_{\lambda}(U)$  shows heavy dependence on the wavelength (relative deviation of  $\pm 21\%$  between 3 and  $16 \mu\text{m}$ ) and a low variability with  $U$  (lower than  $\pm 4\%$ ). It is worth noting that the spectral dependence of  $b_{\lambda}(U)$  shows the same shape as the sea surface reflectivity, i.e.  $1 - \varepsilon_{\lambda}(\theta)$  for a plane sea surface (Masuda *et al.* 1988), as a consequence of the water refractive index spectrum (see figure 4).

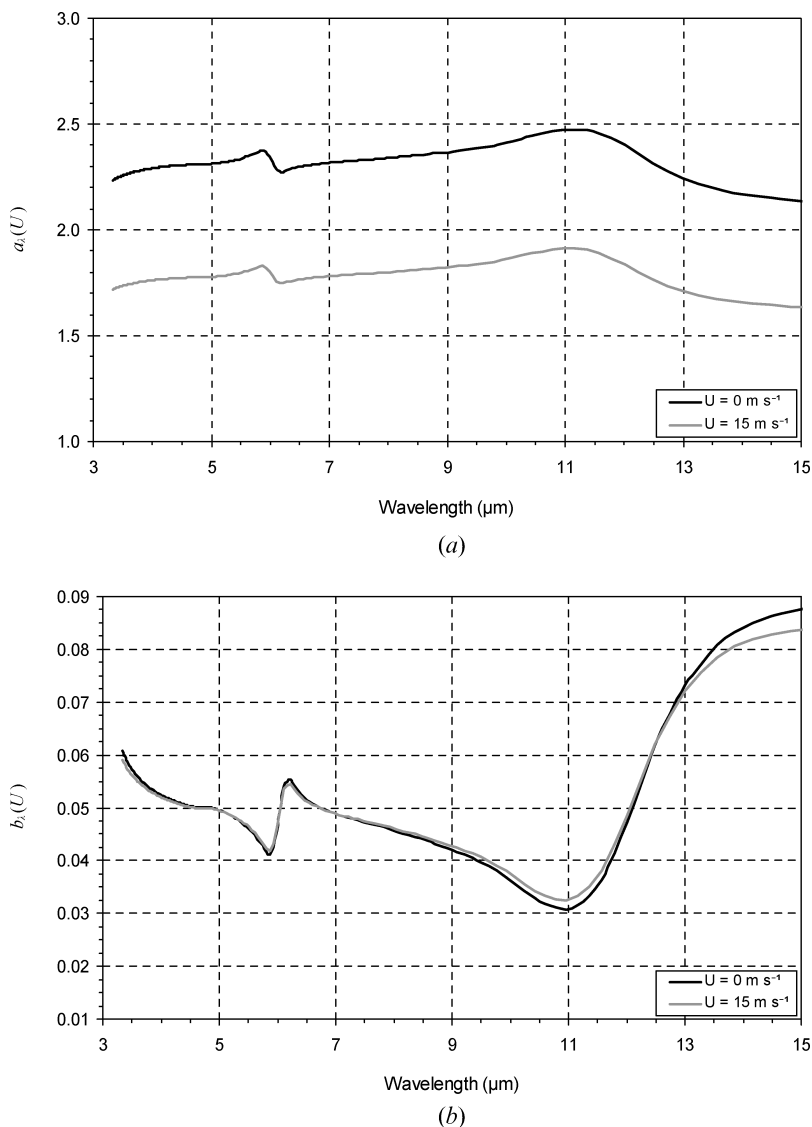


Figure 3. Spectral dependence of the fitting coefficients of equation (4),  $a_\lambda(U)$  and  $b_\lambda(U)$ , for wind speed values of 0 and  $15 \text{ m s}^{-1}$ .

Therefore, the dependence of  $\varepsilon_\lambda(\theta, U)$  on wavelength is just the opposite of that shown by  $b_\lambda(U)$  (see figures 2 and 3(b)). This fact means that the spectral dependence of  $\varepsilon_\lambda(\theta, U)$  is larger for larger observation angles (figure 2), which is in agreement with the results of the model of Wu and Smith (1997) and the experimental data.

Figure 5 shows the spectral dependence of the relative decrease of SSE from nadir to  $55^\circ$ ,  $\left(\frac{\Delta\varepsilon}{\varepsilon}\right)_\lambda = \frac{\varepsilon_\lambda(0^\circ) - \varepsilon_\lambda(55^\circ, U)}{\varepsilon_\lambda(0^\circ)}$ , together with  $b_\lambda(U)$ . The angular decrease is spectrally correlated with  $b_\lambda(U)$ , showing that the effect of this parameter in equation (4) is to increase the spectral SSE dependence with the observation angle, since  $b_\lambda(U)$  is in turn inversely correlated with  $\varepsilon_\lambda(\theta, U)$ . For instance,  $\varepsilon_{11\mu\text{m}}(0^\circ) > \varepsilon_{15\mu\text{m}}(0^\circ)$ , but  $b_{11\mu\text{m}} < b_{15\mu\text{m}}$  and so  $\left(\frac{\Delta\varepsilon}{\varepsilon}\right)_{11\mu\text{m}} < \left(\frac{\Delta\varepsilon}{\varepsilon}\right)_{15\mu\text{m}}$  (see figures 2, 3(b) and 5).

3.2 Adaptation to channel-integrated values

This spectral study demonstrated the good performance of the proposed equation for any wavelength within the mid-wave and long-wave IR. Since all radiometers

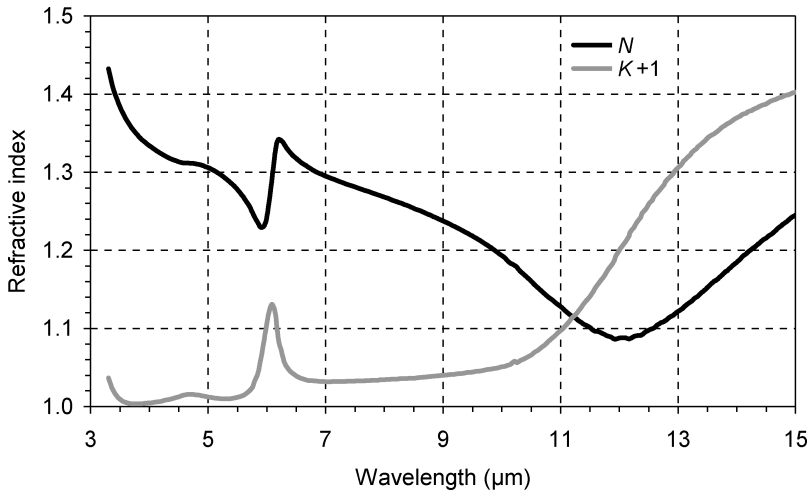


Figure 4. Spectral variation of the complex refractive index,  $n=N-iK$ , for pure water. The real part,  $N$ , is obtained from Hale and Querry (1973) and the imaginary part,  $K$ , from Segelstein (1981). The Friedman (1969) corrections for sea water, which are also spectrally dependent, produce only a slight increase of about 0.005 in  $N$  and a decrease of about 0.002 in  $K$ .

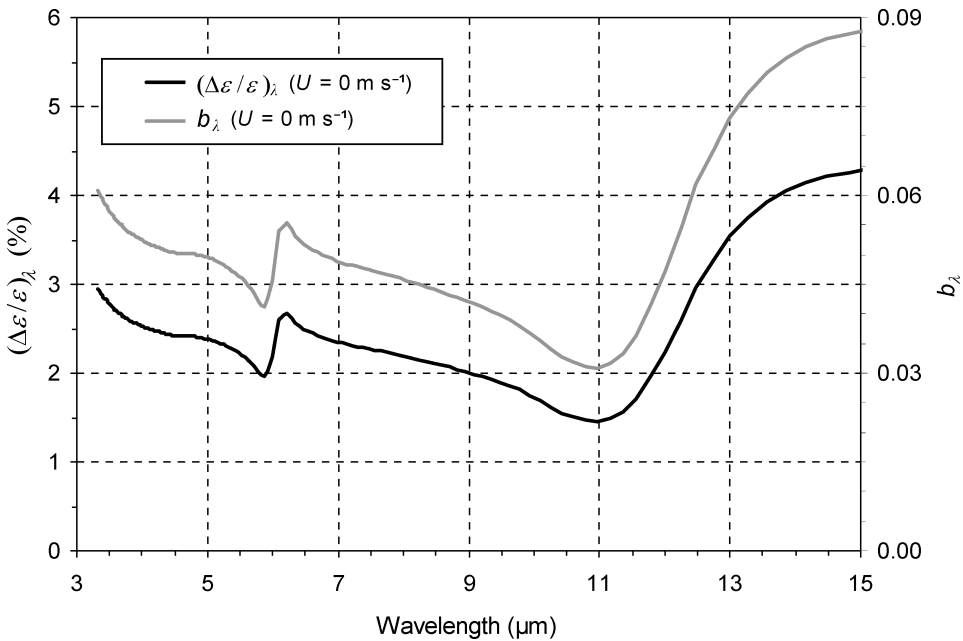


Figure 5. Spectral dependence of the relative SSE decrease from  $0^\circ$  to  $55^\circ$ ,  $\left(\frac{\Delta \epsilon}{\epsilon}\right)_\lambda$ , for  $U=0 \text{ m s}^{-1}$ .  $b_\lambda(U)$  spectral values are also shown for comparison.

measure radiance within spectral bands, rather than single wavelengths, the following step was to check equation (4) for finite-width channels. Therefore, equation (4) was similarly rewritten for a channel  $i$  as:

$$\varepsilon_i(\theta, U) = \varepsilon_i(0^\circ) \left[ \cos(\theta^{a_i(U)}) \right]^{b_i(U)}, \quad (5)$$

where  $\varepsilon_i(\theta, U)$  and  $\varepsilon_i(0^\circ)$  are now SSE values integrated within a spectral band  $i$  from the computed spectral values and  $a_i(U)$  and  $b_i(U)$  are fitting coefficients for the considered band. The SSE values calculated with the model of Wu and Smith (1997) were used again to check the validity of equation (5) for obtaining the SSE for a spectral band in the IR region. The SSE values for a defined channel were obtained by convolution of the spectral SSEs of Wu and Smith (1997) with its normalized filter function. First, SSEs were calculated for the particular IR bands of three sensors: MSG-SEVIRI, EOS Aqua-MODIS and the multi-channel radiometer CE 312. The SEVIRI channels were selected as representative of the usual spectral bands placed in the IR region, since they are similar to the bands of sensors such as AVHRR-NOAA and AATSR-ENVISAT. The MODIS bands were chosen because of their full coverage of the IR atmospheric windows. The CE 312 radiometer was used by the authors (Nicolòs *et al.* 2005) in order to check and prove the soundness of the model of Wu and Smith (1997). This radiometer has similar bands to the SEVIRI's (channel effective wavelengths of 8.82, 10.80 and 11.96  $\mu\text{m}$ . See the effective wavelengths for the SEVIRI channels in table 1). The use of the CE 312 bands allowed us to check the parametrization results, comparing them with the CE 312 measurements (Nicolòs *et al.* 2005) and the emissivities calculated using the model of Wu and Smith (1997), showing a good agreement.

The channel SSEs calculated for wind speed values from 0 to 15  $\text{m s}^{-1}$  were fitted to equation (5) obtaining standard errors,  $\sigma_{f,i}$ , lower than  $\pm 0.0007$  in emissivity for all bands. These values proved the soundness of this equation for finite bands within the IR windows. Figure 6 shows the angular dependence of the SSEs given by equation (5) for the SEVIRI-MSG spectral channels located at 3.9, 8.7, 10.8 and 11.9  $\mu\text{m}$  for 0 and 15  $\text{m s}^{-1}$ , in comparison with the integrated values provided by the model of Wu and Smith (1997).

The analysis of the  $a_i(U)$  and  $b_i(U)$  values confirmed again the assumption of unique wind speed dependence for  $a_i(U)$  and spectral dependence for  $b_i(U)$ . Figure 7 shows the  $b_i(U)$  parameters obtained for the SEVIRI-MSG spectral channels and wind speed from 0 to 15  $\text{m s}^{-1}$ , together with the spectral variation of  $b_i(U)$  for  $U=0 \text{ m s}^{-1}$ . This figure can help to understand why a lower  $b_i(U)$  value was obtained for channels with effective wavelengths around 11  $\mu\text{m}$ , and gives an idea of which values can be expected for satellite channels centred at other wavelengths within the IR. Notice the small variability of  $b_i(U)$  with wind speed, which can be neglected.

### 3.3 The algorithm simplification

The unique dependence of the algorithm on  $U$  is introduced by the coefficient  $a_i(U)$ . Taking into account the low variability of  $a_i(U)$  coefficients with the different spectral channels, we considered an average value of these parameters for each wind speed,  $a(U)$ . A linear regression between  $a(U)$  and  $U$ ,  $a(U) = c U + d$ , yielded a slope of  $c = -0.037 \pm 0.003 \text{ s m}^{-1}$ , and an intercept value of  $d = 2.36 \pm 0.03$ . The regression error

Table 1. Equation(6) parameters for the IR bands of AATSR, AVHRR/2, AVHRR/3, SEVIRI and MODIS (both on EOS Aqua and Terra).  $\lambda_{\text{eff},i}$  is the channel effective wavelength,  $\sigma_{r,i}$  is the fit standard error and  $R_i^2$  is the coefficient of determination.

	Channel	$\lambda_{\text{eff},i}$ ( $\mu\text{m}$ )	$\varepsilon_i(0^\circ)$	$\sigma(\varepsilon_i(0^\circ))$	$b_i$	$\sigma(b_i)$	$\sigma_{r,i}$	$R_i^2$
AATSR (ENVISAT)	IR 3.7	3.74	0.97468	0.00006	0.0550	0.0019	0.0010	0.997
	IR 11	10.86	0.99199	0.00003	0.0343	0.0015	0.0008	0.996
	IR 12	12.05	0.98778	0.00005	0.0508	0.0019	0.0009	0.997
AVHRR/2 (NOAA 14)	3	3.77	0.97495	0.00006	0.0548	0.0019	0.0010	0.997
	4	10.79	0.99174	0.00003	0.0347	0.0015	0.0008	0.996
	5	12.00	0.98823	0.00005	0.0498	0.0019	0.0009	0.997
AVHRR/3 (NOAA 16) (NOAA 17) (NOAA 18)	3B	3.72	0.97440	0.00006	0.0553	0.0019	0.0010	0.997
		3.76	0.97483	0.00006	0.0549	0.0019	0.0010	0.997
	4	3.77	0.97494	0.00006	0.0549	0.0019	0.0010	0.997
		10.92	0.99192	0.00003	0.0348	0.0015	0.0008	0.996
		10.81	0.99184	0.00003	0.0346	0.0015	0.0008	0.997
	5	10.79	0.99187	0.00003	0.0344	0.0015	0.0008	0.996
		11.99	0.98835	0.00005	0.0493	0.0019	0.0009	0.997
		11.93	0.98887	0.00005	0.0480	0.0018	0.0009	0.997
		12.02	0.98807	0.00005	0.0503	0.0019	0.0009	0.997
	SEVIRI (MSG)	4	3.92	0.97613	0.00006	0.0539	0.0019	0.0010
7		8.71	0.98482	0.00005	0.0449	0.0017	0.0008	0.997
9		10.79	0.99176	0.00005	0.0347	0.0015	0.0008	0.996
10		11.94	0.98875	0.00003	0.0483	0.0018	0.0009	0.997
MODIS (Aqua) (Terra)	20	3.78	0.97527	0.00006	0.0546	0.0019	0.0010	0.997
		3.78	0.97535	0.00006	0.0546	0.0019	0.0010	0.997
	21	3.99	0.97687	0.00006	0.0533	0.0019	0.0010	0.997
		3.99	0.97694	0.00006	0.0532	0.0019	0.0010	0.997
	22	3.98	0.97681	0.00006	0.0533	0.0019	0.0010	0.997
		3.97	0.97681	0.00006	0.0533	0.0019	0.0010	0.997
	23	4.07	0.97733	0.00006	0.0529	0.0018	0.0010	0.997
		4.04	0.97725	0.00006	0.0530	0.0018	0.0010	0.997
	24	4.47	0.97891	0.00006	0.0514	0.0018	0.0009	0.997
		4.47	0.97897	0.00006	0.0514	0.0018	0.0009	0.997
	25	4.55	0.97907	0.00006	0.0513	0.0018	0.0009	0.997
		4.55	0.97911	0.00006	0.0512	0.0018	0.0009	0.997
	29	8.56	0.98439	0.00005	0.0455	0.0017	0.0008	0.997
		8.53	0.98432	0.00005	0.0456	0.0017	0.0008	0.997
	31	11.02	0.99229	0.00003	0.0342	0.0015	0.0008	0.996
		11.02	0.99229	0.00003	0.0342	0.0015	0.0008	0.996
32	12.04	0.98813	0.00005	0.0508	0.0019	0.0009	0.997	
	12.03	0.98823	0.00005	0.0506	0.0019	0.0009	0.997	

of the estimate of  $a(U)$  using this linear equation was  $\pm 0.03$  (about  $\pm 1.5\%$ ) and the coefficient of determination was 0.989. Figure 8 shows  $a(U)$  as a function of  $U$ .

Consequently, equation (5) was simplified to:

$$\varepsilon_i(\theta, U) = \varepsilon_i(0^\circ) \left[ \cos(\theta^{(c U + d)}) \right]^{b_i}, \tag{6}$$

where  $b_i$  is a function of the considered spectral band and  $a(U)$  has been replaced with  $a(U) = c U + d$ , where  $c$  and  $d$  are the constant coefficients given above.

In order to test the approximation assumed for  $a(U)$ , channel-dependent values were also considered in equation (6),  $a_i(U) = c_i U + d_i$ , but no significant improvement was obtained in the algorithm accuracy.

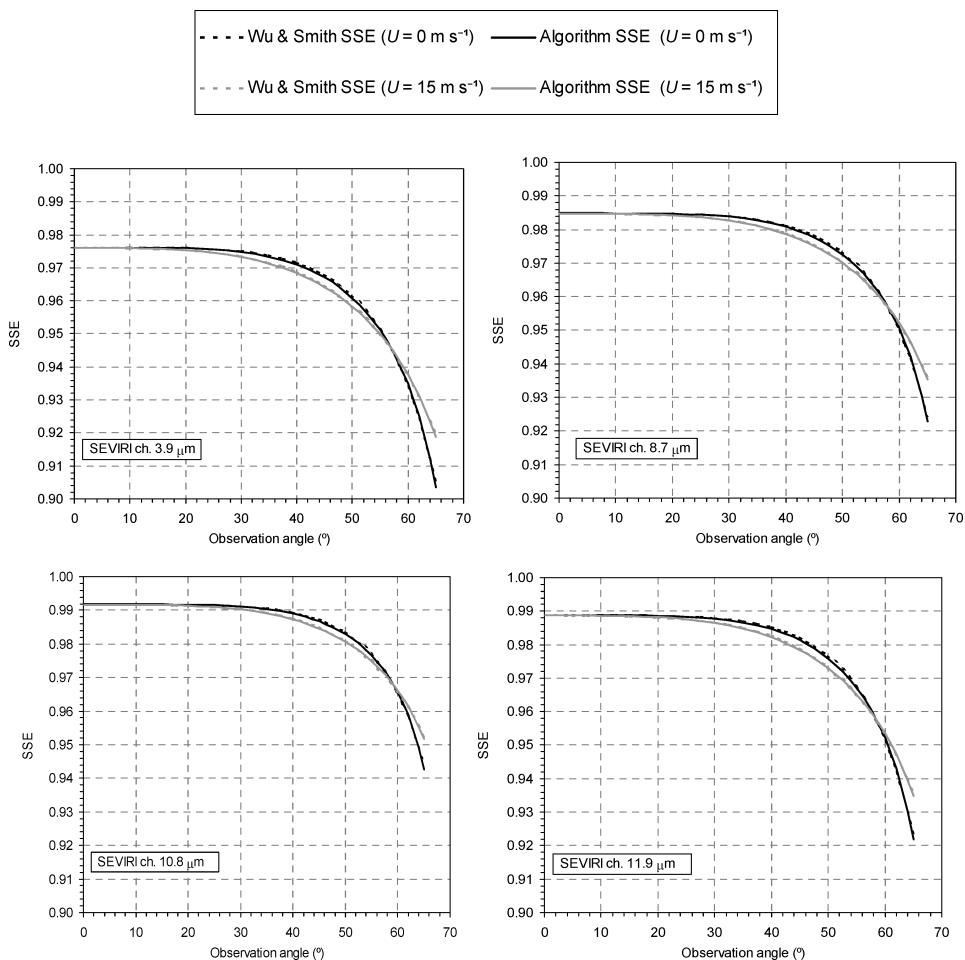


Figure 6. Comparison of the SSE estimations using the model of Wu and Smith (1997) and the SSE values determined by equation (5), with the corresponding parameters for each channel of the SEVIRI (MSG). Both SSEs are integrated values for the IR channels of this sensor, which have effective wavelengths of 3.92, 8.71, 10.79 and 11.94  $\mu\text{m}$ , respectively.

#### 4. Results

Applying equation (6) to several sensor channels and wind speed values, and using the obtained parameters  $c$  and  $d$ ,  $b_i$  was recalculated for each spectral channel. Fit standard errors,  $\sigma_{f,i}$ , lower than  $\pm 0.0009$  were obtained in this case.

Average values of  $b_i$  can be considered for each spectral channel due to the light dependence of this coefficient on  $U$ . Table 1 shows the  $b_i$  parameters obtained for the IR channels of AATSR, AVHRR/2 and AVHRR/3 (NOAA 14 to NOAA 18), MODIS (Terra and Aqua) and SEVIRI. It is worth noting that we only include the coefficients for the spectral bands placed in the spectral windows where radiance measurements can be used for SST retrieval by means of atmospheric and SSE corrections. The corresponding errors,  $\sigma(b_i)$ , are the standard deviations of the  $b_i$  values obtained for the different wind speed conditions, which are always larger than the parameter fit standard deviations. The small  $\sigma(b_i)$  values again show the negligible wind speed dependence for  $b_i$ .

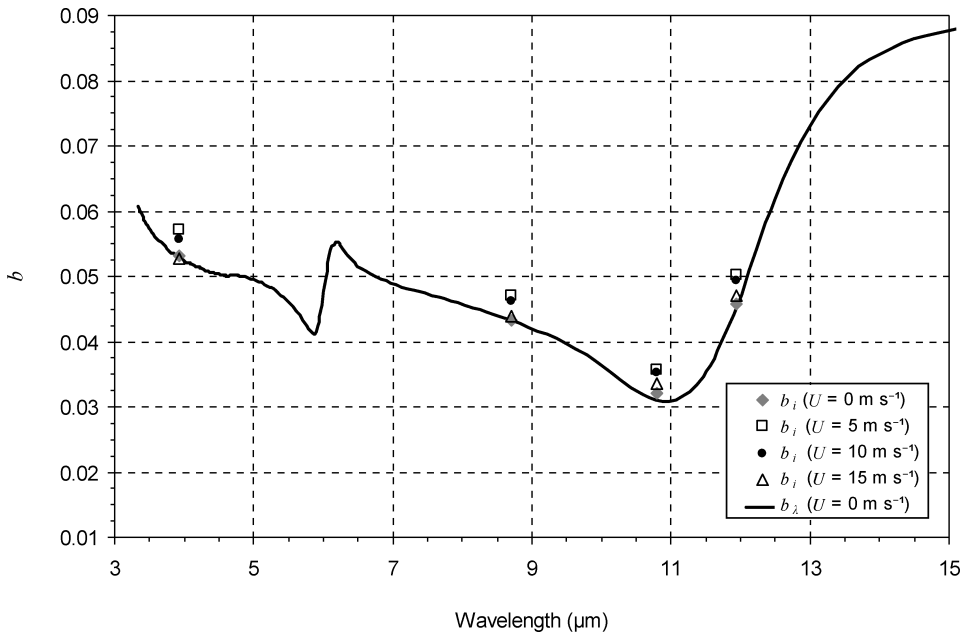


Figure 7.  $b_i(U)$  parameters for the SEVIRI-MSG IR channels and several wind speed values from 0 to  $15 \text{ m s}^{-1}$ , together with the spectral dependence of this parameter for  $U=0 \text{ m s}^{-1}$  as an example.

The input  $\varepsilon_i(0^\circ)$  of equation (6) can be determined using the model of Wu and Smith (1997) at nadir. This is the case for the integrated values included in table 1. The error  $\sigma(\varepsilon_i(0^\circ))$  in table 1 is just the standard deviation of the values obtained for wind speeds from 0 to  $15 \text{ m s}^{-1}$  using this model. However, the input  $\varepsilon_i(0^\circ)$  can

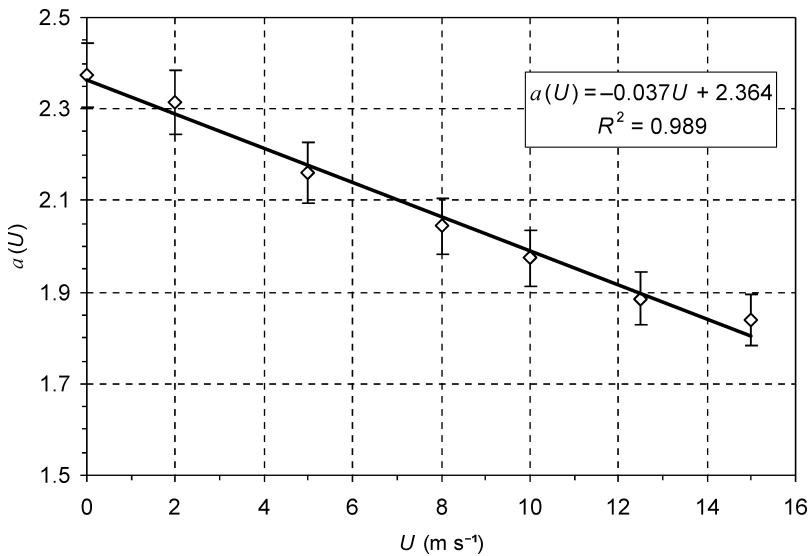


Figure 8. Average values of the  $a_i(U)$  coefficients of equation (5),  $a(U)$ , as a function of  $U$ , together with the linear regression.

be directly measured at nadir by users, or it can also be obtained from spectral emissivity databases, such as the ASTER library (<http://speclib.jpl.nasa.gov/>). Channel values calculated from spectral SSEs of the ASTER library, which were measured in the laboratory using a sample of sea water, differ from the  $\varepsilon_i(0^\circ)$  values of table 1 by approximately  $\pm 0.0010$ , with this value being slightly dependent on the spectral band. Moreover, differences of  $\pm 0.0015$  are obtained from the comparison of CIMEL integrated emissivities determined using the model of Wu and Smith (1997), the spectral values of the ASTER library and the measurements of Nicolòs *et al.* (2005). These differences are lower than the measurement accuracy of  $\pm 0.004$ . Any of these possibilities can be used to determine this input without modifying the emissivity angular variation, which follows the proposed equation.

In the case of SSE determination for the MODIS channels, which have 10 detectors per band with different filter functions for each one, the integration was performed as:

$$\varepsilon_i(\theta, U) = \frac{1}{10} \sum_{J_i=1}^{10} \frac{\int \varepsilon_\lambda(\theta, U) f_{J_i, \lambda} d\lambda}{\int f_{J_i, \lambda} d\lambda}, \quad (7)$$

where  $\varepsilon_i(\theta, U)$  is the SSE for the MODIS channel  $i$ ,  $\varepsilon_\lambda(\theta, U)$  is the monochromatic SSE, and  $f_{J_i, \lambda}$  is the filter function for the  $J$  detector of the  $i$ th band.

Equation (6) was used to determine  $\varepsilon_i(\theta, U)$  for  $\theta \in [0, 65]^\circ$  and  $U \in [0, 15] \text{ m s}^{-1}$ , with the  $b_i$  and  $\varepsilon_i(0^\circ)$  values provided in table 1, as well as the constant  $c$  and  $d$  parameters ( $c = -0.037 \pm 0.003 \text{ s m}^{-1}$  and  $d = 2.36 \pm 0.03$ ), in order to check the accuracy of the parametrization for each channel. The maximum observation angle of  $65^\circ$  was chosen as the angular threshold for which the model of Wu and Smith (1997) was previously validated (Nicolòs *et al.* 2005). These results were compared to the SSE computed through channel integration of the values of the model of Wu and Smith (1997). Low standard errors were obtained, proving the soundness of this simplified algorithm (see the final two columns of table 1). Overall, the estimated error of the parametrization provided by equation (6) is lower than  $\pm 0.0010$  for any channel. The lowest error is introduced for those channels at 9 and 11  $\mu\text{m}$ . Additionally,  $\sigma(\varepsilon_i(0^\circ))$  is minimum for channels at around 11  $\mu\text{m}$ , proving the soundness of this spectral band for the SSE determination, and therefore for the SST retrieval, as discussed in previous work (Nicolòs *et al.* 2004).

A sensitivity analysis was carried out to evaluate the effect of the uncertainty of each input of equation (6). The square emissivity error,  $\sigma_{\text{total}, i}^2$ , can be considered as the square sum of the uncertainties due to the parametrization fit error,  $\sigma_{f, i}^2$ , and the uncertainties of the SSE estimates at nadir,  $u(\varepsilon_i(0^\circ))^2$ ; the surface wind speed,  $u(U)_i^2$ ; and the observation angle,  $u(\theta)_i^2$ , as follows:

$$\sigma_{\text{total}, i}^2 = \sigma_{f, i}^2 + u(\varepsilon_i(0^\circ))^2 + u(\theta)_i^2 + u(U)_i^2, \quad (8)$$

where  $u(x) = (\varepsilon(\theta, U)/x) \sigma(x)$ , with  $x$  being each of the input parameters.

Figure 9 shows a comparison of the contribution of each uncertainty to the total emissivity error. We considered errors of  $\sigma(U) = \pm 1 \text{ m s}^{-1}$  and  $\sigma(\theta) = \pm 0.00175 \text{ rad}$  ( $\pm 1^\circ$ ) for wind speed and observation angle, respectively; the fit error,  $\sigma_{f, i}$  and the errors of  $\varepsilon_i(0^\circ)$  and  $\sigma(\varepsilon_i(0^\circ))$  are given in table 1.

The main source of uncertainty of the proposed equation is the fit error, as the rest of the terms have a negligible effect. Therefore, the total emissivity error can

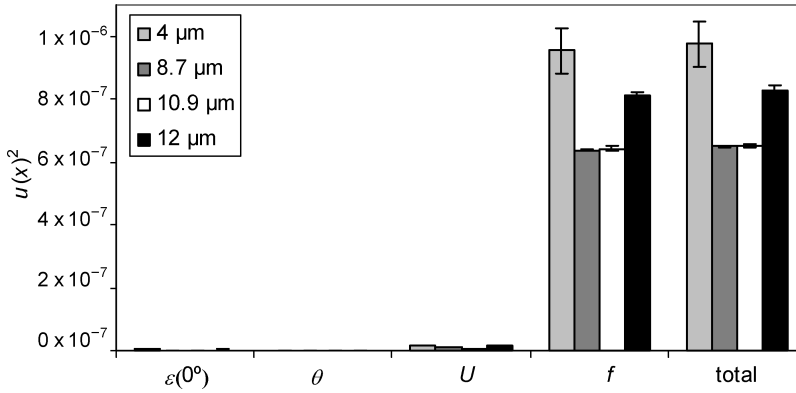


Figure 9. Uncertainty terms of equation(8) grouped by spectral bands, i.e. for band effective wavelengths of around 4, 8.7, 10.9 and 12 μm (see table 1). Bars give the average values for each group and the error bars show standard deviations.

be approximated to the fit error included in table 1, with a maximum error of ±0.0010.

Finally, two SST algorithms have been analysed to determine the effect of this error on the SST retrieval: the single-channel equation and the split-window technique.

The emissivity correction in a single-channel algorithm can be written in terms of temperature as (Coll and Caselles 1994, Coll *et al.* 1994):

$$\Delta T_{EC\_SCi}(\theta, W, U) = \frac{1 - \varepsilon_i(\theta, U)}{\varepsilon_i(\theta, U)} f_i(\theta, W), \tag{9}$$

where  $f_i(\theta, W)$  is a coefficient that depends on the spectral band,  $i$ , surface temperature,  $T_{i,SURF}(\theta)$ , and atmospheric properties,  $T_{i,atm}^\downarrow(\theta, W)$  and  $\tau_i(\theta, W)$ , which are dependent on the column water vapour content,  $W$ :

$$f_i(\theta, W) = \frac{T_{i,SURF}(\theta)}{n_i} + \left[ \frac{n_i - 1}{n_i} T_{i,SURF}(\theta) - T_{i,atm}^\downarrow(\theta, W) \right] (1 - \tau_i(\theta, W)), \tag{10}$$

where  $\tau_i(\theta)$  is the atmospheric transmittance and  $T_{i,atm}^\downarrow(\theta)$  is the effective atmospheric temperature in the downward direction (McMillin 1975). The parameter  $n_i$  is a channel-dependent radiometric parameter (Price 1984), which is obtained from the potential approximation of the Planck function:  $B_i(T) = m_i T^{n_i}$ .

The error in SST due to an error in the emissivity can be obtained as follows:

$$u_{SST\_SC, i}(\varepsilon_i(\theta, U)) = \left| \frac{\partial \Delta T_{EC\_SCi}(\theta, W, U)}{\partial \varepsilon_i(\theta, U)} \right| \sigma(\varepsilon_i(\theta, U)) = \frac{1}{\varepsilon_i(\theta, U)^2} f_i(\theta, W) \sigma(\varepsilon_i(\theta, U)). \tag{11}$$

Equations(9) to (11) were calculated for the AVHRR channel 4 as an example, for which  $n_4 = 4.70535 \pm 0.00013$ . A cloud-free, latitude equally distributed database of 402 radiosoundings (SAFREE; François *et al.* 2002) was used to determine the atmospheric magnitudes involved in the coefficient  $f_4(\theta, W)$ . The radiative transfer code MODTRAN 4 (Berk *et al.* 1999) was used to simulate the atmospheric magnitudes for angles up to 65° and then  $f_4(\theta, W)$  was calculated for the AVHRR. Equation(11) was applied using this coefficient, together with emissivity values for

this sensor and wind speeds from 0 to 15 m s<sup>-1</sup>. An SST error of  $\pm 0.04$  K with a standard deviation of  $\pm 0.009$  K can be obtained as a consequence of the estimated SSE error when a single-channel algorithm is used.

The emissivity correction in the split-window technique can be written in terms of temperature as (Coll and Caselles 1994, Coll and Caselles 1997):

$$\Delta T_{\text{EC\_SW}_i}(\theta, W) = \alpha(W)(1 - \varepsilon(\theta)) - \beta(W)\Delta\varepsilon(\theta), \quad (12)$$

where  $\varepsilon(\theta) = (\varepsilon_4(\theta) + \varepsilon_5(\theta))/2$ ;  $\Delta\varepsilon = \varepsilon_4(\theta) - \varepsilon_5(\theta)$ ; and  $\alpha(W)$  and  $\beta(W)$  are coefficients dependent on the atmospheric properties, which were calculated for the atmospheric profiles from the SAFREE database. In this case, the error in SST due to an error in the emissivity can be again obtained by the propagation of errors as follows:

$$u_{\text{SST\_SW}}(\varepsilon(\theta, U)) = \left[ \left[ \sigma(\varepsilon_4(\theta, U))^2 + \sigma(\varepsilon_5(\theta, U))^2 \right] \left[ (\alpha^2/4) + \beta^2 \right] \right]^{1/2}. \quad (13)$$

In this case, an SST error of  $\pm 0.08$  K with a standard deviation of  $\pm 0.03$  K is obtained. Therefore, the effect of the SSE estimate error when the proposed parametrization is used on the SST determination is relatively low, and is considerably lower than the required accuracy of  $\pm 0.3$  K for SST.

## 5. Summary and conclusions

Current satellite missions use off-nadir observations of IR radiance in both along-track and across-track directions. This fact, together with the high-accuracy requirement for SST satellite measurements, demands accurate IR SSE determinations under any viewing geometry, including those large observation angles at which the SSE shows a significant decrease.

A previous study of the SSE dependence on the observation angle and the sea surface roughness, carried out using in situ measurements (Nicolòs *et al.* 2005), allowed us to compare the soundness of the existing IR SSE models. We concluded that the model of Wu and Smith (1997) accurately reproduced the experimental SSEs for any roughness and observation conditions, but the significant complexity of this model was also highlighted.

The aim of this paper was to develop an algorithm based on the model of Wu and Smith (1997) to easily determine accurate SSEs as a function of the wind speed and the observation angle, whilst avoiding the complexity of the original model. The algorithm was developed through the proposal of an initial spectral parametrization, its adaptation to actual IR bands and a final simplification in order to give an operational equation. The spectral parametrization, given by equation (4), whose coefficients  $a_\lambda(U)$  and  $b_\lambda(U)$  were shown in figure 3, can be used for spectral radiative transfer modelling. The final channel-dependent parametrization (equation (6)) allows the retrieval of channel SSEs from the value at nadir using only three coefficients, from which only one depends on the spectral channels under consideration. The SSEs obtained have an average standard error of estimate of  $\pm 0.0009$ . The parametrization was adapted for several satellite sensors, and the coefficients are provided for their IR bands. The objective is to give channel SSEs that can be used in the split-window technique, with terms depending on the emissivities of the two split-window channels for the emissivity correction (Nicolòs *et al.* 2007a).

The application of this parametrization to satellite imagery of wind speed will permit the production of SSE maps for each IR spectral band. The SSE will be calculated on a pixel-by-pixel basis accounting for the variable observation angle, as well as the possible variation of wind speed. Imagery of wind speed is provided by microwave sensors such as the Advanced Synthetic Aperture Radar (ASAR) on board ENVISAT together with AATSR, the Advanced Microwave Scanning Radiometer for EOS (AMSR-E) on EOS Aqua together with MODIS, the Advanced Scatterometer (ASCAT) on board MetOp-A together with AVHRR/3, the altimeter Poseidon-2 on Jason-1, and the scatterometer QuikScat of NASA (free data available on <http://www.ssmi.com>). The SSE maps generated using wind speed data could be used to determine SST more accurately using, for example, split-window techniques.

In addition, notice that the difference between SSEs provided by the model of Wu and Smith (1997) and the values obtained using the proposed parametrization for 0 and  $15 \text{ m s}^{-1}$  is lower than 0.5% for angles up to approximately  $60^\circ$  (Wu and Smith 1997). For this reason, our parametrization introduces a real simplification within the angular range, where the SSE shows light dependence on wind speed, since although viewing geometry of remote sensing measurements is available, surface wind speed maybe difficult to determine for each IR radiance image due to problems with overlapping. However, wind speed data could improve the SSE estimates, especially for large observation angles.

The implementation of this SSE parametrization in future split-window or dual-angle algorithms for satellite SST retrieval could improve accuracy of that currently required for climate and oceanography investigations. Currently, the inclusion of functions of the form  $f(\sec(\theta)-1)$  in multi-channel algorithms is very common, with this expression being related to the increase of the atmospheric optical path with the observation angle, or to the decrease of the SSE with the angle, depending on the study. A regression analysis of the angular dependence of the SSE against terms  $\sec(\theta)-1$  shows better fitting results when more polynomial terms are taken into account. Consequently, it could be considered as the sum of a polynomial series expansion with terms  $\sec(\theta)-1$ , which is equivalent to a Maclaurin series of a cosine function raised to an exponent. This is the expression of the parametrization proposed in this work by means of a simple observation of the physical dependences of the SSE. However, our equation also includes the wind speed effect, which is important for off-nadir viewings. Therefore, the use of this parametrization in multi-channel algorithms could improve the SST determination from images acquired with large observation angles. In addition, it could be used not only in multi-channel techniques, but also in single-channel and dual-angle algorithms.

### Acknowledgements

This work was supported by the Spanish Ministerio de Educación y Ciencia (project CGL-2004-06099-C03-01/CLI, Acciones complementarias CGL2004-0166-E and CGL2006-27067-E and research contract 'Juan de la Cierva' received by R. Niclòs), the Generalitat Valenciana (project GV2004-B-084) and the University of Valencia (research grant 'V Segles' of J.M. Sánchez). Moreover, we would like to thank Dr P. van Delst (NOAA/NCEP/EMC, Camp Springs MD, USA), who provided us with the computed spectral emissivities of the model of Wu and Smith (1997) that were required for developing the parametrization proposed in this work.

## References

- AMINOU, D.M.A., OTTENBACHER, A., JACQUET, B. and KASSIGHIAN, A., 1999, Meteosat second generation: on-ground calibration, characterisation and sensitivity analysis of SEVIRI imaging radiometer. In *Proceedings, SPIE: Earth Observing Systems IV*, Colorado, USA (International Society for Optical Engineering), **3750**, pp. 419–430.
- BARNES, W.L., PAGANO, T.S. and SALOMONSON, V.V., 1998, Prelaunch characteristics of the Moderate Resolution Imaging Spectroradiometer (MODIS) on EOS-AM1. *IEEE Transactions in Geoscience and Remote Sensing*, **36**, pp. 1088–1100.
- BARTON, I.J., 1992, Satellite-derived sea surface temperatures – a comparison between operational, theoretical and experimental algorithms. *Journal of Applied Meteorology*, **31**, pp. 432–442.
- BERK, A., ANDERSON, G.P., ACHARYA, P.K., CHETWYND, J.H., BERNSTEIN, L.S., SHETTLE, E.P., MATTHEW, M.W. and ADLER-GOLDEN, S.M., 1999, *MODTRAN 4 User's Manual*. Air Force Research Laboratory, Space Vehicles Directorate, Air Force Materiel Command, Hascom AFB, MA, USA.
- COLL, C. and CASELLES, V., 1994, Analysis of the atmospheric and emissivity influence on the split-window equation for sea surface temperature. *International Journal of Remote Sensing*, **15**, pp. 1915–1932.
- COLL, C., CASELLES, V., SOBRINO, J.A. and VALOR, E., 1994, On the atmospheric dependence of the split-window equation for land surface temperature. *International Journal of Remote Sensing*, **15**, pp. 105–122.
- COLL, C. and CASELLES, V., 1997, A split-window algorithm for land surface temperature from advanced very high resolution radiometer data: validation and algorithm comparison. *Journal of Geophysical Research*, **102**, pp. 16697–16713.
- FRANÇOIS, C. and OTTLÉ, C., 1994, Estimation of the angular variation of the sea surface emissivity with the ATSR/ERS-1 data. *Remote Sensing of Environment*, **48**, pp. 302–308.
- FRANÇOIS, C., BRISSON, A., LEBORGNE, P. and MARSOUIN, A., 2002, Definition of a radio-sounding database for sea surface brightness temperature simulations: applications to sea surface temperature retrieval algorithm determination. *Remote Sensing of Environment*, **81**, pp. 309–326.
- FRIEDMAN, D., 1969, Infrared characteristics of ocean water (1.5–15 $\mu$ m). *Applied Optics*, **8**, pp. 2073–2078.
- HALE, G.M. and QUERRY, M.R., 1973, Optical constants of water in the 200 nm to 200  $\mu$ m wavelength region. *Applied Optics*, **12**, pp. 555–563.
- LEGRAND, M., PIETRAS, C., BROGNIEZ, G., HAEFFELIN, M., ABUHASSAN, N.K. and SICARD, M., 2000, A high-accuracy multiwavelength radiometer for in situ measurements in the thermal infrared. Part 1: characterization of the instrument. *Journal of Atmospheric and Oceanic Technology*, **17**, pp. 1203–1214.
- LLEWELLYN-JONES, D., EDWARDS, M.C., MUTLOW, C.T., BIRKS, A.R., BARTON, I.J. and TAIT, H., 2001, AATSR: global-change and surface-temperature measurements from ENVISAT. *ESA Bulletin*, **February**, pp. 11–21.
- MASUDA, K., TAKASHIMA, T. and TAKAYAMA, Y., 1988, Emissivity of pure and sea waters for the model sea surface in the infrared window regions. *Remote Sensing of Environment*, **48**, pp. 302–308.
- McMILLIN, L.M., 1975, Estimation of sea surface temperatures from two infrared window measurements with different absorption. *Journal of Geophysical Research*, **80**, pp. 5113–5117.
- MORÉ, J.J., 1977, The Levenberg–Marquardt algorithm: implementation and theory. Numerical analysis. *Lecture Notes in Mathematics 630*, G.A. Watson (Ed.), pp. 105–116.
- NATIONAL OCEANIC ATMOSPHERIC ADMINISTRATION (NOAA), 2006, *NOAA KLM User's Guide*, J. Robel (Ed.), National Environmental Satellite, Data, and Information Service, NCDC, Asheville, North Carolina, USA.

- NICLÒS, R., CASELLES, V., COLL, C. and VALOR, E., 2004, Autonomous measurements of sea surface temperature using in situ thermal infrared data. *Journal of Atmospheric and Oceanic Technology*, **21**, pp. 683–692.
- NICLÒS, R., VALOR, E., CASELLES, V., COLL, C. and SANCHEZ, J.M., 2005, In situ angular measurements of thermal infrared sea surface emissivity – validation of models. *Remote Sensing of Environment*, **94**, pp. 83–93.
- NICLÒS, R., CASELLES, V., COLL, C. and VALOR, E., 2007a, Determination of sea surface temperature at large observation angles using an angular and emissivity dependent split-window equation. *Remote Sensing of Environment*, **111**, pp. 107–121.
- NICLÒS, R., CASELLES, V., VALOR, E. and COLL, C., 2007b, Foam effect on the sea surface emissivity in the 8–14 $\mu$ m region. *Journal of Geophysical Research*, **112**, p. C12020.
- PRICE, J.C., 1984, Land surface temperature measurements from the split-window channels of the NOAA 7 AVHRR. *Journal of Geophysical Research*, **89**, pp. 7231–7237.
- SEGELSTEIN, D.J., 1981, The complex refractive index of water. MS Thesis, University of Missouri. Kansas City, Missouri, USA.
- SMITH, W.L., KNUTESON, R.O., REVERCOMB, H.E., FELTZ, W., HOWELL, H.B., MENZEL, W.P., NALLI, N.R., BROWN, O., BROWN, J., MINNETT, P. and MCKEOWN, W., 1996, Observations of the infrared radiative properties of the ocean – implications for the measurement of sea surface temperature via satellite remote sensing. *Bulletin of American Meteorological Society*, **77**, pp. 41–50.
- VAN DELST, P.F.W. and WU, X., 2000, A high resolution infrared sea surface emissivity database for satellite applications. In *Technical Proceedings of the Eleventh International ATOVS Study Conference*, Budapest, Hungary, pp. 407–411.
- WATTS, P.D., ALLEN, M.R. and NIGHTINGALE, T.J., 1996, Wind speed effects on sea surface emission and reflection for the along track scanning radiometer. *Journal of Atmospheric and Oceanic Technology*, **13**, pp. 126–141.
- WU, X. and SMITH, W.L., 1997, Emissivity of rough sea surface for 8–13  $\mu$ m: modelling and verification. *Applied Optics*, **36**, pp. 2609–2619.